IEEE Access
Multidisciplinary | Rapid Review | Open Access Journal

Date of publication xxxx 00, 0000, date of current version xxxx 00, 0000.

Digital Object Identifier 10.1109/ACCESS. 2017.Doi Number

Enhancing Classification Accuracy of Transhumeral Prosthesis: A Hybrid sEMG and fNIRS approach

Neelum Yousaf Sattar[1], Zareena Kausar[1], Member, IEEE, Syed Ali Usama, Student Member, IEEE[1], Noman Naseer[1], Senior Member, IEEE, Umer Farooq[1], Ahmed Abdullah[1], Syed Zahid Hussain[1], Umar Shahbaz Khan[2], Haroon Khan[3] and Peyman Mirtaheri[3]

[1]Department of Mechatronics and Biomedical Engineering, Air University, Islamabad, Pakistan
[2] Department of Mechatronics Engineering, CEME, NUST, Rawalpindi, Pakistan
[3]Department of Mechanical, Electronics and Chemical Engineering, OsloMet—Oslo Metropolitan University, Oslo, Norway

Corresponding author Neelum Yousaf Sattar (e-mail: neelum.yousaf@mail.au.edu.pk).

This work was supported by the Higher Education Commission of Pakistan H.E.C under Grant NRPU #10702.

ABSTRACT Limited non-invasive transhumeral prosthesis control exists due to the absence of signal sources on amputee residual muscles. This paper introduces a hybrid brain-machine interface (hBMI) that integrates surface electromyography (sEMG) and functional near-infrared spectroscopy (fNIRS) signals to overcome the limits of existing myoelectric upper-limb prosthesis. This hybridization aims to improve classification accuracy (CA) to escalate arm movements' control performance for individuals who have transhumeral amputation. To evaluate the effectiveness of this hBMI, fifteen healthy and three transhumeral amputee subjects for six arm motions were participating in the experiment. Myo armband was used to acquire sEMG signals corresponding to four arm motions: elbow extension, elbow flexion, wrist pronation, and wrist supination. Whereas fNIRS brain imaging modality was used to monitor cortical hemodynamics response from the prefrontal cortex region for two hand motions: hand open and hand close. The average accuracy of 94.6 % and 74% was achieved for elbow and wrist motions by sEMG for healthy and amputated subjects, respectively. Simultaneously, the fNIRS modality showed an average accuracy of 96.9% and 94.5% for hand motions of healthy and amputated subjects. This study demonstrates the feasibility of hybridizing sEMG and fNIRS signals to improve the CA for transhumeral amputees, improving the control performances of multifunctional upper-limb prostheses.

INDEX TERMS Classification accuracy, fNIRS, hybrid brain-machine interface, sEMG, transhumeral prosthesis.

I. INTRODUCTION

Human arm amputation causes substantial functional and muscle losses for amputees. Transhumeral prosthetic arms are worn by an amputee who suffered from above elbow amputation [1]. For transhumeral amputation, at least three degrees of freedom (DOF) should be available for prosthetic arm's smooth functionality: elbow flexion-extension, forearm pronation-supination, and hand open-close. Nevertheless, the transhumeral amputees do not have sufficient residual muscles to control multiple DOF [2]. The dexterity of control is restricted and ultimately a low acceptance percentage in prosthetic device users [3]. Both invasive and non-invasive procedures exist to control the upper limb prosthesis. The invasive approach typically involves surgical implantation of biosensors such as intramuscular electromyography (iEMG) [4], intracranial electroencephalography (iEEG), electrocorticography (ECoG) [5], and target muscle reinnervation (TMR) [6]. All of them require complex surgical processes to be performed for microelectrode implantation. It lays the foundation for the human-machine interface (HMI) and has been exceptionally effective in accomplishing control of upper limb prosthetic arms [7]. However, these procedures are far from perfect options, as all of them are invasive procedures and include significant risks. Whereas for non-invasive method, scientists have used several biosensors such as surface electromyography (sEMG) [8, 9], electroencephalography (EEG) [10], sonomyography

This article has been accepted for publication in a future issue of this journal, but has not been fully edited. Content may change prior to final publication. Citation information: DOI 10.1109/ACCESS.2021.3099973, IEEE Access

(SMG) [11], near-infrared (NIR) [12], functional near-infrared spectroscopy (fNIRS) [13], mechanomyography (MMG) [14, 15], and force myography (FMG) [16].

For several decades, sEMG signals are investigated as an intuitive HMI to control prosthetic arms [17, 18]. It gives information about muscle activity by placing an electrode on the skin's surface [18-20]. It is preferred due to the ease of signal extraction procedure and non-invasive technique. In addition to that, external sensory inputs from switches, kinematic features, gyroscopes, pressure sensors, visual servoing [21], and inertial measurement unit (IMU) [22] are also used to control prostheses [23]. Despite the vast and favored application of sEMG, one of the biggest challenges is extracting proper sEMG signals from human biceps and triceps to detect muscle intention and generate a control command. This is due to less available residual muscle for transhumeral amputation. Also, signal degradation due to muscular fatigue and proneness to crosstalk from neighboring muscles is observed [24, 25]. Combining sEMG with other complementary sensor modalities is beneficial for improved upper-limb prosthesis control [8, 26-28]. Thus, it has been proposed to combine myoelectric signals with other bio-signals and name it as hybrid myoelectric control systems [29]. Three significant aims of hybridization are to improve the classification accuracy (CA), to increase the number of control commands, and decrease the time to detect the bio-signal [30]. Presently, non-invasive hybrid brain-machine interface (hBMI) technologies are abundantly used to achieve hybridization goals for prosthetic limb control. Combining EEG and EMG is a promising technique to control exoskeletons and prosthetic devices [27]. This scheme attains a decent control performance even in the presence of muscular fatigue [31]. The obtained EEG signals are not perfect due to signal acquisition difficulties, low rate of data transfer, achieved accuracy, and little user flexibility [26, 29].

Additionally, EMG and kinematic signals are combined to assess the CA of eight arm movements in transhumeral amputees. However, the kinematic signals are susceptible to motion artifact [32]. An integrated hybrid system is also developed for simultaneous EMG and MMG measurement [14]. This platform captured muscular activations in different frequencies tested on able-bodied and trans-radial amputees. Its results suggested that MMG-assisted myoelectric sensing can improve control performance. An sEMG/NIRS hybrid system is developed to combine the advantages of EMG and NIRS to fulfill the requirements of adequate upper limb prosthesis control. It is tested on healthy subjects and trans-radial amputees [29]. Buccino et al [33] reported the control performance of an EEG-fNIRS hybrid sensor system to discriminate between a set of motor tasks. The obtained CA of the hybrid sensor system is higher than the accuracy achieved from individual modality (EEG or fNIRS), but they proposed this scheme on limited arm motions. It is evident from the available literature that most of the hBMI schemes are applied to control transradial prosthesis. However, little work is done to control the above-elbow amputations [2, 34], indicating a significant shortcoming [35].

This research proposes an hBMI solution to control six different arm motions for transhumeral amputees. A hybrid combination of two non-invasive modalities: sEMG and fNIRS, is presented. The acquired signals from both modalities were processed, and different features were tested on a classifier to generate control commands. As per the authors' best knowledge, the presented hBMI approach for transhumeral amputation and its analysis have never been reported earlier. Section 2 presents materials and methods used: data acquisition, signal processing, channel selection, feature extraction, and classification. Whereas, in section 3, results are presented and discussed before concluding the work.

II. MATERIALS AND METHODS

In this section, all information related to the experimental protocol followed by details of methodology used in signal acquisition, signal processing, classification, and hybridization framework are included.

A. DATA ACQUISITION

1) SUBJECTS

For this study, fifteen healthy subjects (age: 20-35) and three transhumeral amputees were recruited. The demographic characteristics of amputees are given in Table I. None of the selected participants had a previous history of any neurological, cardio-respiratory, or visual ailment. All of the subjects had normal or corrected to normal vision. The subjects were also educated in detail about the experimental process, and all subjects gave their written consent. None of the amputees was using any prosthetic device. The experiments were conducted following the latest Declaration of Helsinki and were approved by the Air University Human Research Ethics Committee (AUHREC)

2) SENSOR PLACEMENT

a) sEMG Armband

For decoding elbow and wrist motion of subjects arm, Myo armband (Thalmic Labs, Canada) is used. It is a wearable gadget provided with eight electromyographic (sEMG) electrodes, a 9-axes inertial measurement unit (IMU) (3-axes gyroscope, 3-axes accelerometer and 3-axes magnetometer) and a transmission module (Myo Armband web site; Thalmic Labs Inc., 2013– 2018). The EMG electrodes detect the signals related to muscles activity of the user's arm. The acquired data are sent via the Bluetooth Low Energy (BLE) module embedded into the armband, other electronic devices (actuators, microcontrollers, and so on), which perform specific functions depending on the received data on their installed software. It is positioned on the biceps of the subjects arm. The armband acquired the sEMG signals for four-arm motions: elbow extension (EE), elbow flexion (EF), wrist pronation (WP), and wrist supination (WS).

This article has been accepted for publication in a future issue of this journal, but has not been fully edited. Content may change prior to final publication. Citation information: DOI 10.1109/ACCESS.2021.3099973, IEEE Access

b) fNIRS Optode Placement

The NIRx Imaging system, NIRsport (NIRx Medical Technologies, Germany), was used to obtain fNIRS signals for two hand motions: hand close (HC) and hand open (HO). The NIRsport is an accessible, segmental, and robust functional near-infrared spectroscopy (fNIRS) machine that measures hemodynamic responses generated by neuro-activation of brain via oxy-, deoxy-, and total hemoglobin variations in the cerebral cortex. Eight sources and eight detectors were positioned on the subjects' brain prefrontal cortex region to record fNIRS signals with a separation of 3 cm between sender and receiver's optodes [27], resulting in twenty-two channels. The sEMG armband and fNIRS optodes placement on amputee A1 are illustrated in Figure 1(a).

3) EXPERIMENTAL PROCEDURE

The experiment comprised of two parts: a training session and a testing session. All subjects were instructed to execute six tasks, among which four tasks were detected by sEMG and two tasks by fNIRS. The experiments were executed in a confined room for the training session to reduce disturbance from the surrounding environment. Each subject was seated in a comfortable chair with their arms placed on armrests. They were also advised to remain relaxed during the experiment to avoid any unnecessary movement or thinking. The training session was initiated with a resting period of 3 mins to establish a data baseline. After completing the rest period, participants received cues of six specific tasks shown on a screen approximately 80 cm away from the subject. The first two tasks were performed to acquire fNIRS signals from the prefrontal region of the subject's brain. It included mental arithmetic (MA): subtraction of two-digit numbers from three-digit numbers in pseudo-random order (e.g., 245 − 22 =?) and word formation (WF): formation of six-letter words (e.g., "Monday"). It is reported that the word-formation signals are weaker than mental arithmetic, and hence these two activities can easily be differentiated from each other, aiding in the classification [21].

The remaining four tasks were executed to acquire sEMG signals, and the subjects were asked to have an initial 5-sec rest followed by a 20-sec task period. This model was implemented for the acquisition of four-arm motions: elbow extension (EE), elbow flexion (EF), wrist pronation (WP), and wrist supination (WS). The information regarding the experimental protocol and data recording process are provided in figure 2.

B. SIGNAL PROCESSING AND CHANNEL SELECTION

The data from both modalities (sEMG and fNIRS) were acquired using the paradigm given in Figure 2. The obtained data set from each sensor was independently processed and filtered to obtain the desired signals.

1) fNIRS SIGNAL PROCESSING

fNIRS data were recorded using NIRports (NIRx Inc.) using two wavelengths 760 nm and 850 nm, respectively. Signal processing and data analysis were carried out using the nirsLAB® software. The fNIRS data were first preprocessed to remove physiological noises [28], and a sampling rate of 7.81 Hz was used to acquire the data. For each experiment, every channel's signal was filtered using a band-pass filter (0.01–0.2 Hz) to reduce the effects of cardiac, respiratory and very low-frequency confounders [29]. The Modified Beer-Lambert Law (MBLL) [21, 30], given in (1), was used to convert changes in raw optical density signals into oxy- and deoxy-hemoglobin concentration changes respectively, $\left(\Delta c_{\mathrm{HbO}}(t) \text{ and } \Delta c_{\mathrm{HbR}}(t)\right)$:

$$\begin{bmatrix} \Delta c_{Hb O}(t) \\ \Delta c_{Hb R}(t) \end{bmatrix} = \frac{\begin{bmatrix} \alpha_{Hb O}(\lambda_1) & \alpha_{Hb O}(\lambda_1) \\ \alpha_{Hb O}(\lambda_2) & \alpha_{Hb O}(\lambda_2) \end{bmatrix}^{-1} \begin{bmatrix} \Delta A(t;\lambda_1) \\ \Delta A(t;\lambda_{12}) \end{bmatrix}}{l \times DPF} \quad (1)$$

In (1), DPF is the curve path length factor, and l is the distance between source and detector. $A(t;\lambda_1)$ and $A(t;\lambda_2)$ is the absorption at two different instants, $\alpha_{HbO}(\lambda)$ and $\alpha_{HbR}(\lambda)$ are the extinction coefficients of HbO and HbR, $\Delta c_{HbO}(t)$ and $\Delta c_{HbR}(t)$ are changes in concentration of HbO and HbR, respectively.

2) sEMG SIGNAL PROCESSING

Myo armband was used to acquire sEMG signals. It is a wearable and resizable device that allows acquiring of sEMG signals from different arm sizes (thin or thick). It includes eight sEMG sensors and a 9-axis inertial measurement unit which contains a gyroscope, an accelerometer, and a magnetometer, three axes each. The armband uses a 200 Hz sampling frequency for signal acquisition. Myo armband was placed on the biceps of the subject's arm while they were sitting. After sensor placement, the armband was connected to a laptop via a USB Bluetooth adapter. Myo diagnostics software was used to display signals in graphical form for each electrode. The signals on this graphical display can be visually inspected for electrodes' signal quality during each specific task. The signals were captured during the experiments using the Myo Capture tool of the software. Myo Capture stored the time series of all the numerical values of voltages obtained from the sensors in an auto-generated Microsoft excel® sheet. The excel sheet held nine columns: eight containing data for eight electrodes and one containing time points. Myo armband extracts data as an analog voltage in millivolts (mV), uses its built-in filters to remove noise(s), and yields noise-free 8-bit data. The output voltages vary between -30mV to +80mV. These voltages are digitized from -128 to 127 and later normalized between -1 and +1 for data processing in MATLAB 2019®. Figure 5 shows the averaged raw signal obtained from eight electrodes of the armband for elbow extension (EE) motion captured from a healthy subject.

This article has been accepted for publication in a future issue of this journal, but has not been fully edited. Content may change prior to final publication. Citation information: DOI 10.1109/ACCESS.2021.3099973, IEEE Access

3) CHANNEL SELECTION

Before features extraction, appropriate electrodes/optodes must be selected if a brain-machine interface (BMI) aims to achieve high CA with minimum complexity. Preceding studies have proposed different methods to select channels or signals for classification, comprising bundled optode-based approaches [31] and t-value based approaches [28]. On the other hand, further studies have employed their own algorithms, for instance, independent component analysis [32]. We used the following criteria to select sEMG and fNIRS electrodes/ optodes.

For sEMG signals, after the signal acquisition of all subjects, the amplitude of each electrode was analyzed. For each electrode, the minimum value of the signal was subtracted from the median value. This difference of values was averaged for all eight electrodes. The averaged values ranged between 48~58 mV for all subjects. Therefore, 48mV was selected as the threshold value to see the channel activation. Any channel with a lesser value than 48mV was discarded. Whereas for fNIRS signals, a channel-averaging approach [33] was used.

C. FEATURE EXTRACTION

To generate six control commands, relevant features for the classification were extracted. For fNIRS signals, peak (SP) and mean (SM) of the signals were selected as features. As per the literature [34] SM and SP provide better control performance for fNIRS-based systems. Also, in consideration of the reported possibility of an initial fNIRS signal dip, a minimum (min) signal value was added as a feature [35]. For sEMG signals, we selected the waveform length (WL) and the number of peaks as features. The features were calculated from only selected electrodes that showed significant activation using a 250 ms moving window. For both modalities (sEMG and fNIRS), MATLAB® was used to implement all the features' computation.

D. CLASSIFICATION

Linear discriminant analysis (LDA) was used to classify the sEMG and fNIRS signals to evaluate the performance of the features. In literature, LDA has been extensively applied to multiclass problems as it results in high performance with low computational cost [36, 37] and faster than the support vector machine [34], motivated the authors to select LDA. The governing Fisher's criteria is given as in (2).

$$J(v) = \frac{v^t S_B\, v}{v^t S_w v} \tag{2}$$

Between classes scatter matrix S_B is defined as in (3):

$$S_B = \sum_{x_i}^{c} n_i\,(\mu_i - \mu)(\mu_i - \mu)^t \tag{3}$$

Where, n_i represents several samples that belong to class i. Whereas, within-class scatter matrix, Sw, is given as (4):

$$S_w = \sum_{x_i}^{c} S_i = \sum_{x_i}^{c} \sum_{x_k \in Classi} (x_k - \mu_i)(x_k - \mu_i)^t \tag{4}$$

Generalized eigenvector problem is represented as (5):

$$S_B v = \lambda S_w v \tag{5}$$

The optimal v is the eigenvector corresponding to the largest eigenvalue. This is represented as (6) provided that S_w is nonsingular.

$$v = S_W^{-1}(\mu_i - \mu) \tag{6}$$

The LDA classifier performance was estimated using 10-fold cross-validation. The whole data was split randomly into ten groups, among which nine were used for training purposes, and the remaining one was used for testing. This entire procedure was repeated ten times till all the groups were tested against each other. However, figure 3 illustrates a hBMI scheme for transhumeral prosthesis control using sEMG and fNIRS.

III. RESULTS

In this study, two signal modalities i.e., sEMG and fNIRS are hybridized to generate six control commands for a transhumeral prosthesis. Figure 4 plots subject 6's selected optode-wise hemodynamics states values for two-hand activities. While performing a brain activity, it was observed that not all channels were active. Chanel 1, 2, 3, 9, 12, and 16 show the activity for word formation, while on channel 18, 19, 20, and 22, the activity from the arithmetic means. In figure 4, the block averages of the selected optodes are illustrated. It is visible that both the tasks are visually separately and hence resulted in higher accuracy. These active channels were used to extract the statistical features which took part in the classification. However, for both mental tasks, the activation pattern seems to appear on the same channels. Thus, there existed a need to select channels that are contributing rather than increasing computational time. In the previous section, a channel-averaging approach was used for channel selection. In our case, the subjects were asked to move their right hand. [28, 38]. However, both these actions appeared in the different regions of the brain that can be identified. The spatial features were calculated, which reflects brain activity in the pre-frontal cortex region.

Window sizing of diverse spans has been utilized in several studies to detect fNIRS features [38-40]. It is intended to minimize the window size to generate a fast response for real-time applications. So, the time spans of 0 – 0.5, 0 – 1, and 0 – 2 seconds windows were selected. These split seconds were employed for EMG features extraction and investigation of hemodynamic features to secure the best window size to decrease calculation time. Figure 5 represents the raw sEMG signals obtained from eight electrodes for elbow extension (EE) motion captured from a healthy subject arm. It can be seen that electrodes 2, 3 and 4 show significant activity as they are positioned on the tricep muscle which is activated for the elbow extension motion.

This article has been accepted for publication in a future issue of this journal, but has not been fully edited. Content may change prior to final publication. Citation information: DOI 10.1109/ACCESS.2021.3099973, IEEE Access

The reported performance measures were computed based on the number of correctly classified samples over the task time (0–10 s) and were evaluated by 10-fold cross-validation. The highest value of accuracy recorded for two-class fNIRS activity was 97% for subject 6 and for sEMG activity, the highest accuracy recorded is 94%. As for the amputees, the fNIRS signals were more expressed compared to the sEMG signals. Hence, the accuracy for two classes of fNIRS was recorded to be 94.6% while sEMG resulted in the accuracy of the highest value of 73%. The accuracies obtained using sEMG and fNIRS for all healthy and amputated subjects are shown in Figure 6.

The offline testing results on the trained modal has been illustrated in Table III. It can be seen that the most mis-classified motions are of hand-open and hand-closed motion as stated earlier in section II, which arise the notion for control command generation using a combination of modalities.

Similarly, as per the experimental design, real-time validation was separated into two types of catagories: Type-1: training and testing with all motions with both signal modalities and 2) Type-2: training with one motion and testing with other motions muscle contraction and hemodynamic response as well. In this strategy, the amputated subject is instructed to perform the activity with different random (can include untrained) intentions at the time of testing. A total of 10 activities have been performed in a randomized manner. For healthy subjects, the number of activities was increased to 20 motions.

1) Type-1: The result of all activities is shown in Table VI. for the amputee-1. The mean CA of ≈ % has been reported. The highest and lowest error rates of 0% and 40% have been seen for the activity EE, EF, HO, HC, WP, and WS. The pattern recognition error is highest 50% for the activity HC when amputee-3 has been considered, as shown in Table IV. The overall classification error of 18%, 11%, and 18.3% has been observed for A1, A2, and A3. For amputee-3, the CA is 88% and the highest error of 40% is seen as shown in Table IV. A similar trend has been observed in offline analysis. This validates the proposed scheme for the real-time application.

Type-2: Testing with the unknown signals resulted in the CA of 25%, 15%, and 25% has been observed when the classification model developed using training with different subjects for A1, A2 and A3 respectively. The results of this experiment are described in Table V.

IV. DISCUSSION

Combining various bio-signals is a potential method to attain abundant neural information for multiple degree prosthesis control. This will aid to decode more accurate motion intention of transhumeral amputees. In this work, to improve the control performances of multi DOF myoelectric prosthetic arm, an hBMI scheme through sEMG and fNIRS signals for hand, wrist and elbow motion identification is studied. The authors combined two non-invasive modalities in the presented research: sEMG and fNIRS to generate six control commands for trans humeral amputee. This study demonstrated the feasibility of fusing sEMG and fNIRS signals towards improving motion classification accuracy for above-elbow amputees, enhancing the control performances of multifunctional myoelectric prostheses in clinical application. It also overcome the specific disadvantages of each individual modality of BMI. This is the first time sEMG and fNIRS signals are combined to generate control command for prosthetic arm control to the best of authors knowledge.

This research's ultimate goal was to control six arm degree motions: EE, EF, WP, WS, HO and HC using non-invasive hBMI. These arm motions are the least prerequisite to maintain the functionality for above elbow amputation. The proposed scheme generates four control commands from sEMG data acquired from biceps and triceps. The obtained average accuracy was 94.6% and 74% for healthy and amputated subjects, respectively. Nevertheless, previous to this study, sEMG data from bicep and triceps of healthy and amputated subjects were also acquired for HO and HC motion. However, quality sEMG signals were not achieved from biceps and triceps of healthy subjects or stumped muscles in amputees. A possible reason would be that when an above-elbow amputee makes a hand motion, the remaining muscles would produce relatively weak sEMG signals. Although these muscles are not functionally associated with the respected hand movements [41]. The obtained classification accuracy of sEMG for six control commands was around 16.4 – 29.3%, not acceptable. Unlike the forearm, the arm, which is the upper limb between the shoulder joint and the elbow joint, has minor muscle activity, and the elbow joint and forearm twist motions cannot be predicted. Therefore, non-invasive signal processing is a big challenge for above elbow amputation, but the state of the artwork shows that hBMI may help resolve such problems. Table 2 shows details of different existing hBMI for upper-limb prosthesis control, whereas the last 5 schemes have been carried out in the last five years. It also includes the presented research results as current work in the last row of the table to compare existing hybrid methods.It is apparent from Table 2 that most of them have carried their experiments for transradial amputee. The obtained results of this research are included in the table 2

Through the proposed scheme, it can be seen that the number of commands is increased, and there is no decrease in the accuracy. When sEMG alone is used, the recorded intentions from hand motion are weak and disturb the system's overall accuracy. Using fNIRS individually does not help much either. As the number of commands increases, the accuracy of the classifier decreases. It is because the hemodynamic patterns take time to reach the baseline after activation. Due to this time delay, which can be of 17s [37], the control command generation accuracy is affected. By using both modalities, this issue was addressed. When the fNIRS response comes back to baseline, the sEMG can predict a

motion that can be translated into a control command. The number of commands is increased as well the accuracy remains above 90%.

For this study, the results were obtained based on offline analysis, and the classification accuracy only evaluated the performances of the proposed hybrid method. In the future, the proposed method's efficiency would be investigated in a real-time environment and assessed by more measures such as motion selection time, motion completion time, and motion completion rate.

VII. CONCLUSION

In this research study, we investigated the prospect of decoding six commands from the subject's biceps and the prefrontal cortices region with better accuracy using hBMI. Hybridization: combining surface electromyography (sEMG) and functional near-infrared spectroscopy (fNIRS) is proposed. Four sEMG control commands were generated, corresponding to two elbows and two wrist movements (EE, EF, WP and WS movements), using the number of peaks and the waveform length as features. Two fNIRS control commands were generated for two hand movements (HO and HC), using the means and peaks of signals as features. For fNIRS, mental arithmetic (MA) and word formation (WF) tasks were chosen for activity decoding. We selected a 0 –2s window and 250ms window for fNIRS and sEMG signals, respectively, to generate six control commands. The signal mean, peak, and minimum values were used to incorporate hemodynamic signals and initial dip features in the classifier. The performed experiments demonstrated the hBMI feasibility and potential applications of the proposed six command decoding scheme. The outcome of this study might help realize the control of multifunctional myoelectric prostheses for above-elbow amputees. Further research on feature selection criteria and increasing the number of control commands to improve the prosthetic arm's controllability. Moreover, the incorporation of adaptive algorithms for prosthetic control and hBMI for motion control can further strengthen the results.

ACKNOWLEDGMENT

This work was supported by the Higher Education Commission of Pakistan H.E.C under Grant NRPU #10702. The authors would also like to thank the faculty of Technology, Art and Design, OsloMet, Norway, to make this collaboration possilbe.

REFERENCES

[1] F. Cordella, A. L. Ciancio, R. Sacchetti, A. Davalli, A. G. Cutti, E. Guglielmelli, and L.Zollo, "Literature review on needs of upper limb prosthesis users," Frontiers in neuroscience, vol. 10, p. 209, 2016.

[2] D. A. Bennett, J. E. Mitchell, D. Truex, and M. Goldfarb, "Design of a Myoelectric Transhumeral Prosthesis," IEEE/ASME Transactions on Mechatronics, vol. 21, pp. 1868-1879, 2016.

[3] J. Ribeiro, F. Mota, T. Cavalcante, I. Nogueira, V. Gondim, V. Albuquerque, and A.Alexandria "Analysis of Man-Machine Interfaces in Upper-Limb Prosthesis: A Review," Robotics, vol. 8, p. 16, 2019.

[4] R. F. Weir, P. R. Troyk, G. A. DeMichele, D. A. Kerns, J. F. Schorsch, and H. Maas, "Implantable myoelectric sensors (IMESs) for intramuscular electromyogram recording," IEEE Transactions on Biomedical Engineering, vol. 56, pp. 159-171, 2009.

[5] T. Pistohl, T. Ball, A. Schulze-Bonhage, A. Aertsen, and C. Mehring, "Prediction of arm movement trajectories from ECoG-recordings in humans," Journal of neuroscience methods, vol. 167, pp. 105-114, 2008.

[6] T. A. Kuiken, G. Li, B. A. Lock, R. D. Lipschutz, L. A. Miller, K. A. Stubblefield, and K.B Englehart, "Targeted muscle reinnervation for real-time myoelectric control of multifunction artificial arms," Jama, vol. 301, pp. 619-628, 2009.

[7] C. Cipriani, J. L. Segil, J. A. Birdwell, and R. F. ff Weir, "Dexterous control of a prosthetic hand using fine-wire intramuscular electrodes in targeted extrinsic muscles," IEEE Transactions on Neural Systems and Rehabilitation Engineering, vol. 22, pp. 828-836, 2014.

[8] N. Jarrassé, C. Nicol, A. Touillet, F. Richer, N. Martinet, J. Paysant, and J.B de Graaf, "Classification of phantom finger, hand, wrist, and elbow voluntary gestures in transhumeral amputees with sEMG," IEEE Transactions on Neural Systems and Rehabilitation Engineering, vol. 25, pp. 71-80, 2016.

[9] A. H. Al-Timemy, R. N. Khushaba, G. Bugmann, and J. Escudero, "Improving the performance against force variation of EMG controlled multifunctional upper-limb prostheses for transradial amputees," IEEE Transactions on Neural Systems and Rehabilitation Engineering, vol. 24, pp. 650-661, 2016.

[10] D. Bandara, J. Arata, and K. Kiguchi, "Towards control of a transhumeral prosthesis with EEG signals," Bioengineering, vol. 5, p. 26, 2018.

[11] Y. Fang, N. Hettiarachchi, D. Zhou, and H. Liu, "Multi-modal sensing techniques for interfacing hand prostheses: a review," IEEE Sensors Journal, vol. 15, pp. 6065-6076, 2015.

[12] C. Jian, L. Deng, L. Liang, J. Luo, X. Wang, and R. Song, "Neuromuscular Control of the Agonist–Antagonist Muscle Coordination Affected by Visual Dimension: An EMG-fNIRS Study," IEEE Access, vol. 8, pp. 100768-100777, 2020.

[13] N. Naseer and K.-S. Hong, "fNIRS-based brain-computer interfaces: a review," Frontiers in human neuroscience, vol. 9, p. 3, 2015.

[14] W. Guo, X. Sheng, H. Liu, and X. Zhu, "Mechanomyography assisted myoelectric sensing for upper-extremity prostheses: A hybrid approach," IEEE Sensors Journal, vol. 17, pp. 3100-3108, 2017.

[15] M. A. Islam, K. Sundaraj, R. B. Ahmad, N. U. Ahamed, and M. A. Ali, "Mechanomyography sensor development, related signal processing, and applications: a systematic review," IEEE Sensors Journal, vol. 13, pp. 2499-2516, 2013.
[16] X. Jiang, L.-K. Merhi, Z. G. Xiao, and C. Menon, "Exploration of Force Myography and surface Electromyography in hand gesture classification," Medical Engineering & Physics, vol. 41, pp. 63-73, 2017.
[17] W. Shahzad, Y. Ayaz, M. J. Khan, N. Naseer, and M. Khan, "Enhanced Performance for Multi-Forearm Movement Decoding Using Hybrid IMU–sEMG Interface," Frontiers in neurorobotics, vol. 13, p. 43, 2019.
[18] A. Phinyomark, R. N Khushaba, and E. Scheme, "Feature Extraction and Selection for Myoelectric Control Based on Wearable EMG Sensors", Sensors, vol. 18, p. 1615, 2018.
[19] C. Loconsole, G. D. Cascarano, A. Brunetti, G. F. Trotta, G. Losavio, V. Bevilacqua, and E. Di Sciascio , "A model-free technique based on computer vision and sEMG for classification in Parkinson's disease by using computer-assisted handwriting analysis," Pattern Recognition Letters, vol. 121, pp. 28-36, 2019.
[20] A. Phinyomark, P. Phukpattaranont, and C. Limsakul, "Feature reduction and selection for EMG signal classification," Expert systems with applications, vol. 39, pp. 7420-7431, 2012.
[21] D. K. Madusanka, R. Gopura, Y. Amarasinghe, and G. K. Mann, "Hybrid vision based reach-to-grasp task planning method for trans-humeral prostheses," IEEE Access, vol. 5, pp. 16149-16161, 2017.
[22] D. A. Bennett and M. Goldfarb, "IMU-based wrist rotation control of a transradial myoelectric prosthesis," IEEE Transactions on Neural Systems and Rehabilitation Engineering, vol. 26, pp. 419-427, 2017.
[23] Z. Ju and H. Liu, "Human hand motion analysis with multisensory information," IEEE/ASME Transactions on Mechatronics, vol. 19, pp. 456-466, 2014.
[24] Z. Ju, G. Ouyang, M. Wilamowska-Korsak, and H. Liu, "Surface EMG based hand manipulation identification via nonlinear feature extraction and classification," IEEE Sensors Journal, vol. 13, pp. 3302-3311, 2013.
[25] D. Farina, N. Jiang, H. Rehbaum, A. Holobar, B. Graimann, H. Dietl, O.C Aszmann, "The extraction of neural information from the surface EMG for the control of upper-limb prostheses: emerging avenues and challenges," IEEE Transactions on Neural Systems and Rehabilitation Engineering, vol. 22, pp. 797-809, 2014.
[26] W. Guo, X. Sheng, H. Liu, and X. Zhu, "Development of a multi-channel compact-size wireless hybrid SEMG/NIRS sensor system for prosthetic manipulation," IEEE Sensors Journal, vol. 16, pp. 447-456, 2016.
[27] T. D. Lalitharatne, K. Teramoto, Y. Hayashi, and K. Kiguchi, "Towards hybrid EEG-EMG-based control approaches to be used in Bio-robotics applications: current status, challenges and future directions," Paladyn, Journal of Behavioral Robotics, vol. 4, pp. 147-154, 2013.
[28] S. Sadeghi and A. Maleki, "Recent advances in hybrid brain-computer interface systems: a technological and quantitative review," Basic and clinical neuroscience, vol. 9, p. 373, 2018.
[29] W. Guo, X. Sheng, H. Liu, and X. Zhu, "Toward an Enhanced Human–Machine Interface for Upper-Limb Prosthesis Control with Combined EMG and NIRS Signals," IEEE Transactions on Human-Machine Systems, vol. 47, pp. 564-575, 2017.
[30] K.-S. Hong and M. J. Khan, "Hybrid brain–computer interface techniques for improved classification accuracy and increased number of commands: a review," Frontiers in neurorobotics, vol. 11, p. 35, 2017.
[31] A. Chowdhury, H. Raza, Y. K. Meena, A. Dutta, and G. Prasad, "An EEG-EMG correlation-based brain-computer interface for hand orthosis supported neuro-rehabilitation," Journal of neuroscience methods, vol. 312, pp. 1-11, 2019.
[32] N. Jiang, I. Vujaklija, H. Rehbaum, B. Graimann, and D. Farina, "Is accurate mapping of EMG signals on kinematics needed for precise online myoelectric control," IEEE Transactions on Neural Systems and Rehabilitation Engineering, vol. 22, pp. 549-558, 2014.
[33] A. P. Buccino, H. O. Keles, and A. Omurtag, "Hybrid EEG-fNIRS asynchronous brain-computer interface for multiple motor tasks," PloS one, vol. 11, p. e0146610, 2016.
[34] G. Gaudet, M. Raison, and S. Achiche, "Classification of upper limb phantom movements in transhumeral amputees using electromyographic and kinematic features," Engineering Applications of Artificial Intelligence, vol. 68, pp. 153-164, 2018.
[35] T. R. Farrell, "A comparison of the effects of electrode implantation and targeting on pattern classification accuracy for prosthesis control," IEEE Transactions on Biomedical Engineering, vol. 55, pp. 2198-2211, 2008.
[36] Q. Zhang, E. N. Brown, and G. E. Strangman, "Adaptive filtering to reduce global interference in evoked brain activity detection: a human subject case study," Journal of biomedical optics, vol. 12, p. 064009, 2007.
[37] M. J. Khan and K.-S. Hong, "Hybrid EEG–fNIRS-based eight-command decoding for BCI: application to quadcopter control," Frontiers in neurorobotics, vol. 11, p. 6, 2017.
[38] M. D. Pfeifer, F. Scholkmann, and R. Labruyère, "Signal processing in functional near-infrared spectroscopy (fNIRS): methodological differences lead to different statistical results," Frontiers in human neuroscience, vol. 11, p. 641, 2018.
[39] A. Zafar, M. J. Khan, J. Park, and K.-S. Hong, "Initial-dip Based Quadcopter Control: Application to fNIRS-BCI," IFAC-PapersOnLine, vol. 51, pp. 945-950, 2018.
[40] H.-D. Nguyen and K.-S. Hong, "Bundled-optode implementation for 3D imaging in functional near-infrared spectroscopy," Biomedical Optics Express, vol. 7, pp. 3491-3507, 2016.
[41] H. Santosa, M. Jiyoun Hong, S.-P. Kim, and K.-S. Hong, "Noise reduction in functional near-infrared spectroscopy signals by independent component analysis," Review of Scientific Instruments, vol. 84, p. 073106, 2013.

[42] M. J. Khan and K.-S. Hong, "Passive BCI based on drowsiness detection: an fNIRS study," Biomedical optics express, vol. 6, pp. 4063-4078, 2015.
[43] K.-S. Hong, N. Naseer, and Y.-H. Kim, "Classification of prefrontal and motor cortex signals for three-class fNIRS–BCI," Neuroscience letters, vol. 587, pp. 87-92, 2015.
[44] A. Zafar and K.-S. Hong, "Detection and classification of three-class initial dips from prefrontal cortex," Biomedical optics express, vol. 8, pp. 367-383, 2017.
[45] Y. Yu, X. Sheng, W. Guo, and X. Zhu, "Attenuating the impact of limb position on surface EMG pattern recognition using a mixed-LDA classifier," in 2017 IEEE International Conference on Robotics and Biomimetics (ROBIO), 2017, pp. 1497-1502.
[46] H. Nazeer, N. Naseer, R. A. A. Khan, F. M. Noori, N. K. Qureshi, U. S. Khan, and , "Enhancing classification accuracy of fNIRS-BCI using features acquired from vector-based phase analysis," Journal of Neural Engineering, 2020.
[47] M. J. Khan and K.-S. J. F. i. n. Hong, "Hybrid EEG–fNIRS-based eight-command decoding for BCI: application to quadcopter control," vol. 11, p. 6, 2017.
[48] E. Demandt, C. Mehring, K. Vogt, A. Schulze-Bonhage, A. Aertsen, and T. Ball, "Reaching movement onset-and end-related characteristics of EEG spectral power modulations," Frontiers in neuroscience, vol. 6, p. 65, 2012.
[49] S. Weyand, K. Takehara-Nishiuchi, T. J. I. T. o. N. S. Chau, and R. Engineering, "Weaning off mental tasks to achieve voluntary self-regulatory control of a near-infrared spectroscopy brain-computer interface," vol. 23, pp. 548-561, 2015.
[50] X. Li, O. W. Samuel, X. Zhang, H. Wang, P. Fang, and G. Li, "A motion-classification strategy based on sEMG-EEG signal combination for upper-limb amputees," Journal of neuroengineering and rehabilitation, vol. 14, pp. 1-13, 2017.
[51] D. Blana, T. Kyriacou, J. M. Lambrecht, and E. K. Chadwick, "Feasibility of using combined EMG and kinematic signals for prosthesis control: a simulation study using a virtual reality environment," Journal of Electromyography and Kinesiology, vol. 29, pp. 21-27, 2016.
[52] O. Barron, M. Raison, G. Gaudet, and S. Achiche, "Recurrent Neural Network for electromyographic gesture recognition in transhumeral amputees," Applied Soft Computing, vol.96, p. 106616, 2020.
[53] C. Lauretti, A. Davalli, R. Sacchetti, E. Guglielmelli, and L. Zollo, "Fusion of M-IMU and EMG signals for the control of trans-humeral prostheses," 6th IEEE International Conference on Biomedical Robotics and Biomechatronics (BioRob), pp. 1123-1128, 2016,.
[54] E. Nsugbe, C. Phillips, M. Fraser, and J. McIntosh, "Gesture Recognition for Trans-humeral Prosthesis Control Using EMG and NIR," IET Cyber-systems and Robotics, vol. 2, pp. 122-131, 2020.
[55] N. A. Alshammary, D. A. Bennett, and M. Goldfarb, "Synergistic elbow control for a myoelectric transhumeral prosthesis," IEEE Transactions on Neural Systems and Rehabilitation Engineering, vol. 26, pp. 468-476, 2017.
[56] F. M. Noori, N. Naseer, N. K. Qureshi, H. Nazeer, and R. A. Khan, "Optimal feature selection from fNIRS signals using genetic algorithms for BCI," Neuroscience letters, vol. 647, pp. 61-66, 2017

.

Tables and Figures:

TABLE I
DEMOGRAPHIC CHARACTERISTICS OF AMPUTEES

Subject ID	Age (years)	Affected Side	Residual stump length	Cause of Amputation	Time since amputation
A1	32 ± 4.83	Right	15 cm	Car Accident	7 months
A2	38 ± 4.83	Right	17 cm	Car Accident	24 months
A3	52 ± 4.83	Right	13 cm	Electric Shock	145 months

This article has been accepted for publication in a future issue of this journal, but has not been fully edited. Content may change prior to final publication. Citation information: DOI 10.1109/ACCESS.2021.3099973, IEEE Access

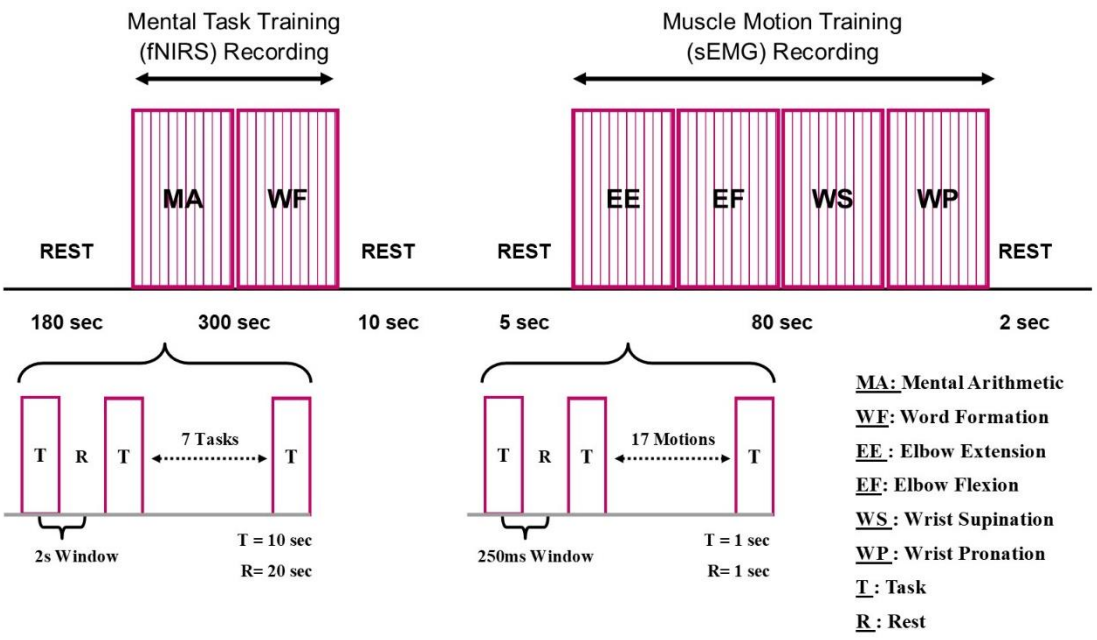

FIGURE 1: Hybrid surface electromyography (Myo armband) and functional near-infrared spectroscopy (optodes placement) setup: (a) amputee A1 while wearing Myo armband on his biceps and NIRSport head cap positioned on his prefrontal region of the brain to acquire

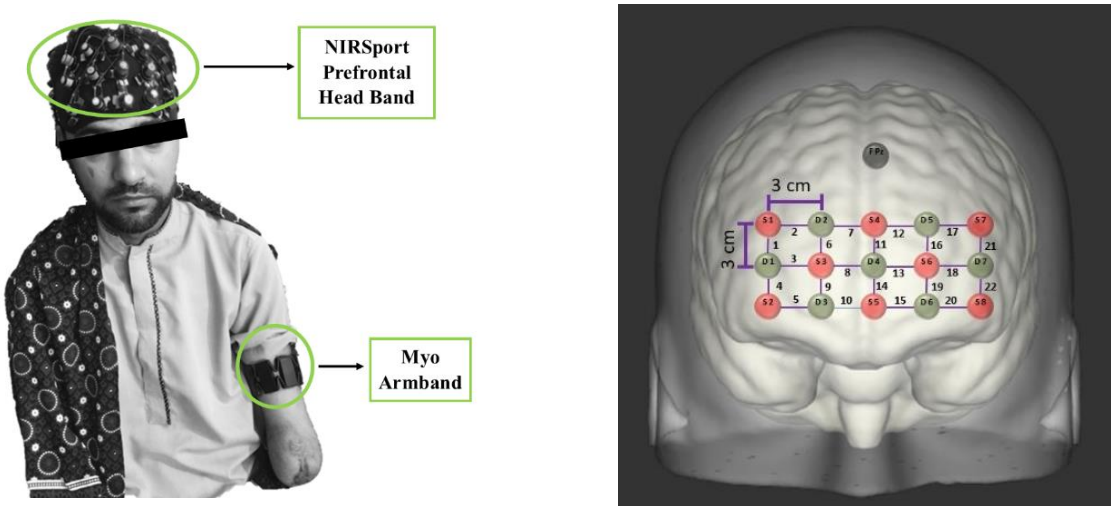

(a) (b)

FIGURE 2. After an initial 3-min rest, each fNIRS block consists of 10-s activations, and 20-s rests, while every surface electromyography block comprises of 1-s activations and 1-s rests. The total experiment duration for acquiring sEMG and fNIRS signals is 11mins

This article has been accepted for publication in a future issue of this journal, but has not been fully edited. Content may change prior to final publication. Citation information: DOI 10.1109/ACCESS.2021.3099973, IEEE Access

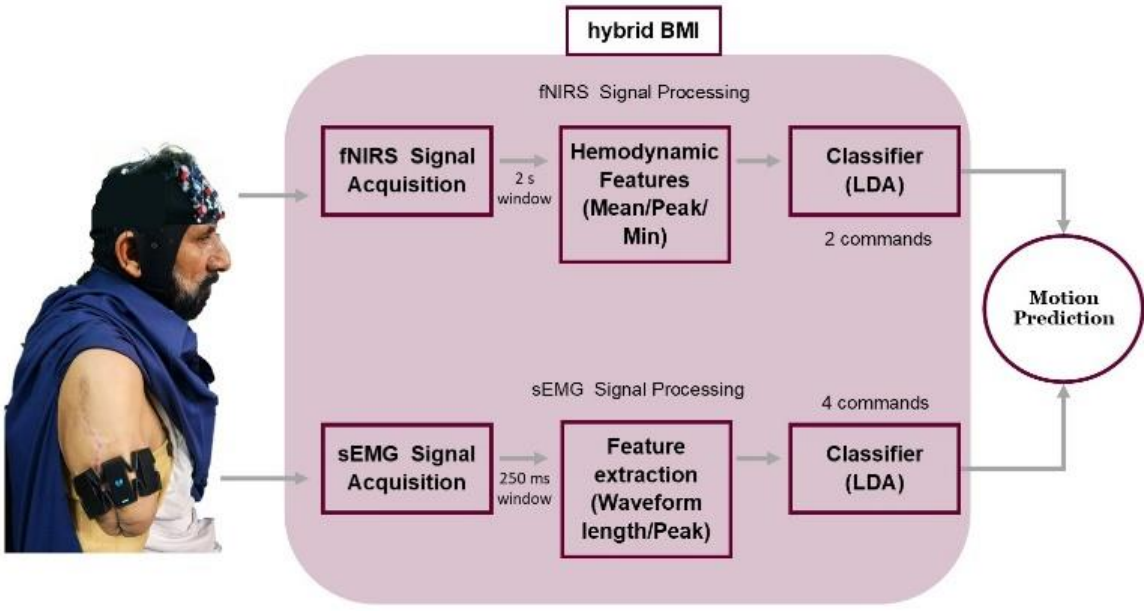

FIGURE 3. **The framework of Hybrid sEMG and fNIRS for Transhumeral Prosthesis Control**

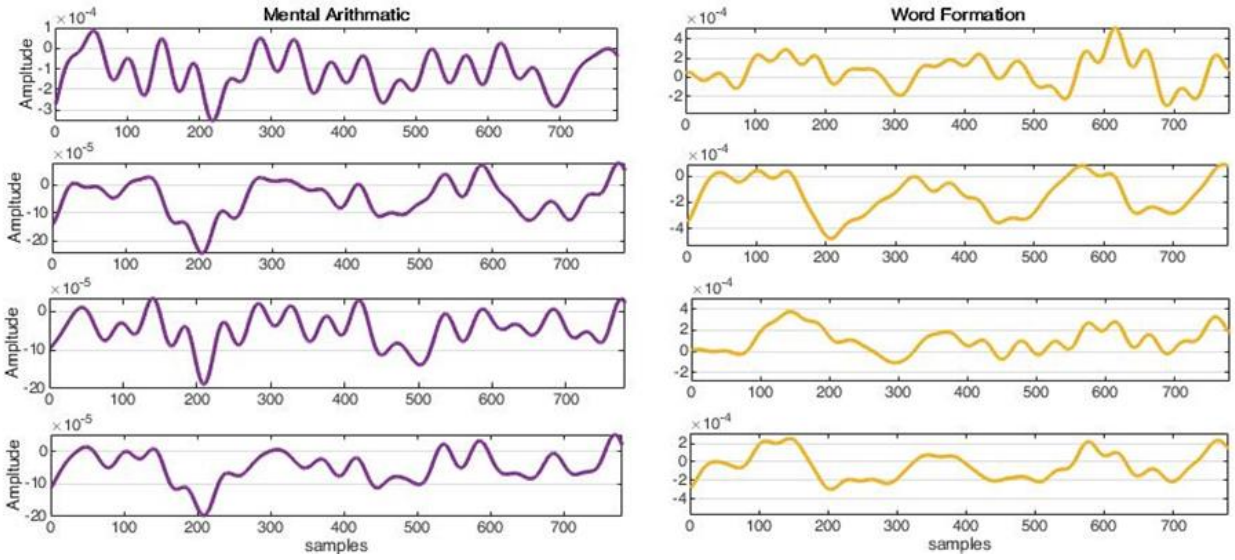

FIGURE 4. **Selected optode-wise hemodynamic states block averaging visualization for both the tasks**

This article has been accepted for publication in a future issue of this journal, but has not been fully edited. Content may change prior to final publication. Citation information: DOI 10.1109/ACCESS.2021.3099973, IEEE Access

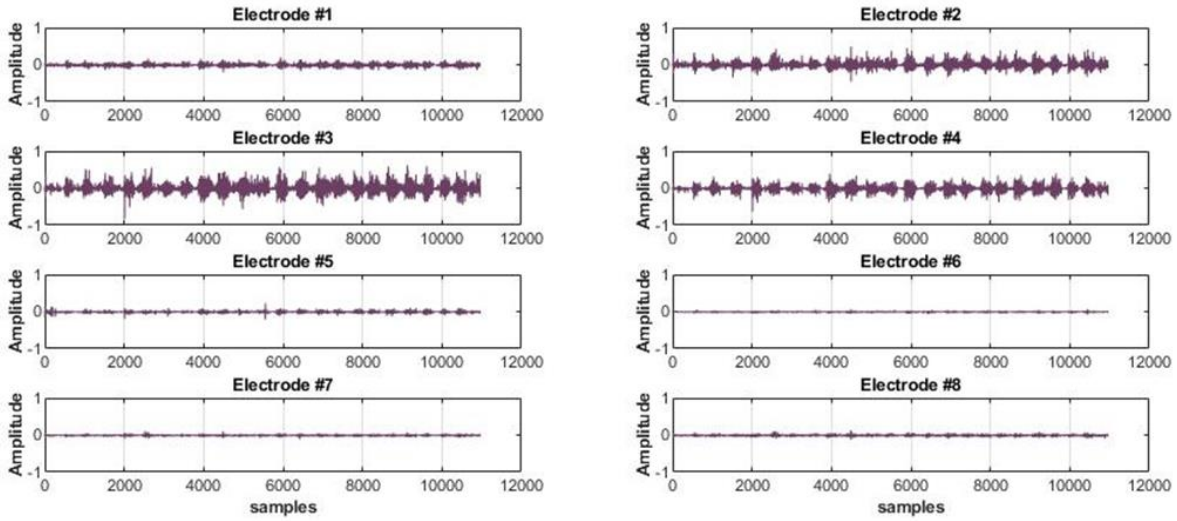

FIGURE 5: Channel/electrode-wise raw sEMG data for elbow extension EE motion captured from a healthy subject

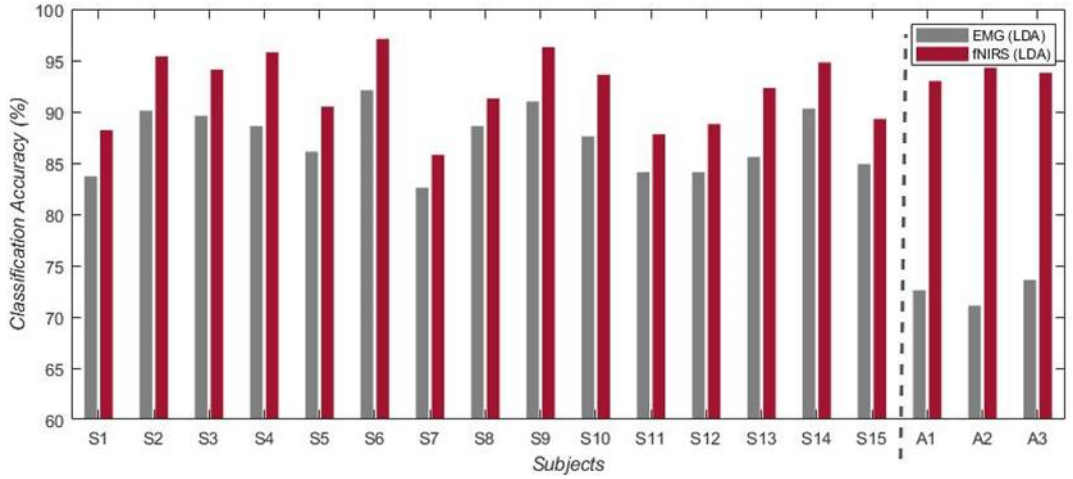

FIGURE 6. Subject wise obtained classification accuracies using sEMG and fNIRS for fifteen healthy subjects are represented as S1 – S15 while amputated subjects are labelled as A1 – A3

This article has been accepted for publication in a future issue of this journal, but has not been fully edited. Content may change prior to final publication. Citation information: DOI 10.1109/ACCESS.2021.3099973, IEEE Access

TABLE II
COMPARISON OF PROPOSED METHOD WITH RECENT HYBRID BRAIN MACHINE INTERFACE BASED ON MODALITY TYPE, SENSOR PLACEMENT, CLASSIFIER, COMMAND GENERATION AND ACCURACY FOR UPPER LIMB PROSTHETIC CONTROL. THE H REPRESENTS HEALTHY SUBJECTS WHILE A FOR AMPUTEES.

Table III: Offline amputee classification results motion-wise

Input Class	No. of Motions	No. of Misclassified samples					
		A1		A2		A3	
		sEMG	fNIRS	sEMG	fNIRS	sEMG	fNIRS
EE	20	0	n/a	0	n/a	0	n/a
EF	20	0	n/a	1	n/a	0	n/a
WS	20	2	n/a	3	n/a	1	n/a
WP	20	2	n/a	2	n/a	3	n/a
HO	20	8	1	4	0	12	2
HC	20	11	1	4	0	9	1

Table IV: Real-time amputee motion-wise accuracy for case #1

Input Class	No. of Motions	No. of Misclassified samples					
		A1		A2		A3	
		sEMG	fNIRS	sEMG	fNIRS	sEMG	fNIRS
EE	10	0	n/a	0	n/a	0	n/a
EF	10	1	n/a	0	n/a	1	n/a
WS	10	2	n/a	1	n/a	0	n/a
WP	10	1	n/a	2	n/a	1	n/a
HO	10	4	1	2	0	4	2
HC	10	3	0	2	0	5	2

Table V: Real-time amputee motion-wise accuracy for case #2

Input Class	No. of Motions	No. of Misclassified samples					
		A1		A2		A3	
		sEMG	fNIRS	sEMG	fNIRS	sEMG	fNIRS
EE	10	0	n/a	0	n/a	1	n/a
EF	10	2	n/a	1	n/a	1	n/a
WS	10	4	n/a	0	n/a	1	n/a
WP	10	1	n/a	3	n/a	2	n/a
HO	10	5	1	3	0	4	2
HC	10	3	0	2	1	6	1